

How Thin Can You Go?

Performance of Thin Copper and Aluminum RF Coil Conductors

*Radim Barta¹, Vyacheslav Volotovskyy², Keith Wachowicz^{1,3}, B. Gino Fallone^{1,3,4},
Nicola De Zanche^{1,3*}*

1. Department of Oncology, Division of Medical Physics, University of Alberta, 11560 University Avenue, Edmonton, Alberta T6G 1Z2, Canada
2. MagnetTx Oncology Solutions Ltd., Edmonton, Alberta T6G 2T5, Canada
3. Department of Medical Physics, Cross Cancer Institute, 11560 University Avenue, Edmonton, Alberta T6G 1Z2, Canada
4. Department of Physics, University of Alberta, Edmonton, Alberta, Canada

* Corresponding Author

Published in

Magnetic Resonance in Medicine

DOI: 10.1002/mrm.28540

Keywords:

alternate conductors, aluminum, efficiency, quality factor, RF coils, SNR, thin conductors

Abstract

Purpose:

To evaluate the impact of emerging conductor technology on radio-frequency (RF) coils. Performance and resulting image quality of thin or alternate conductors (e.g., aluminum instead of copper) and thicknesses (9–600 μm) are compared in terms of signal-to-noise ratio (SNR).

Methods:

Eight prototype RF coils (15 cm \times 15 cm square loops) were constructed and bench tested to measure quality factor (Q). The coils used 6 mm wide conducting strips of either copper or aluminum of a few different thicknesses (copper: 17, 32, 35, 127, 600 μm ; aluminum: 9, 13, 20, 127 μm) on acetate projector sheets for backing. Corresponding image SNR was measured at 0.48 T (20.56 MHz).

Results:

The coils spanned a range of unloaded quality factors from 89 to 390 and a five-fold range of losses. The image SNRs were consistent with the coils' bench-measured efficiencies (0.33 to 0.73). Thin aluminum conductors (9 μm) led to the highest reduction in SNR (65% that of 127 μm copper). Thin copper (<32 μm) conductors lead to a much smaller decrease in SNR (approximately 10%) compared to 127 μm copper. No performance difference was observed between 127 μm thick copper and aluminum. The much thicker 600 μm copper bars only yield a 5% improvement in SNR.

Conclusion:

Even at 0.48 T copper RF coil conductors much thinner than those in conventional construction can be used while maintaining SNR greater than 50% that of thick copper. These emerging coil conductor technologies enable RF coil functionality that cannot be achieved otherwise.

1) Introduction

Several emerging technologies are expanding the range of conductors available for RF coils beyond traditional materials. In conventional RF coil construction, thick copper conductors (including solid or hollow bars or tubes, as well as standard printed circuit boards (PCB)) ensure the coil has the lowest possible losses for a given design due to copper's excellent electrical conductivity ($5.9 \times 10^8 \text{ Sm}^{-1}$) [1]. Resistive losses in the conductor lead to lower SNR [2]; therefore traditional coil design has naturally placed an emphasis on minimizing losses. Use of conductors several times thicker than the skin depth is necessary to avoid SNR losses due to sub-optimal current cross-section [3].

Recent RF coil design paradigms, however, relax this convention to take advantage of the benefits of thin or alternate conductor coils. For example, lightweight, flexible coils are more comfortable [4] and can provide better SNR than rigid setups due to closer proximity to the imaging region. Examples include screen-printing to create RF coils that are incorporated into infant blankets [4], as well as flexible, meandering wires that allow the coil conductor's path to change [5,6]. Conductive textiles can be stretched up to a 100 times their size [7], and a flexible coil made from a conductive elastomer based on silver microparticles achieves an SNR just 14% lower than a reference copper coil [8]. Liquid metal [9,10] and braided conductors [11] also allow for stretchable coils that closely fit moving and flexing body parts [9,11]. Further alternate conductors include aluminum (conductivity $3.54 \times 10^8 \text{ Sm}^{-1}$), which has applications in multi-modality systems such as X-ray MRI [12], PET-MRI [13], and linac-MR systems [14,15], where interactions with ionizing radiation must be minimized. In X-ray MRI [12], aluminum coils significantly reduce artifacts in the X-ray image compared to the copper coils. In PET-MRI [13], attenuation of the photons through aluminum is reduced compared to copper, but the difference is inconsequential because the required correction is equally effective for copper or aluminum conductors. In linac-MR systems [14,15], the use of aluminum conductor of the same thickness as copper leads to interactions with the beam that are up to three times smaller.

Thinner conductors can also allow for reduced interactions with radiation [14], as well as allowing form-fitting coils made of flexible PCB (which use thinner copper than the up to $70 \mu\text{m}$ typically used in rigid PCBs). Quantifying the increased resistance expected due to using a thinner conductor is, however, not simple analytically. For thin rectangular traces both the classical and

lateral skin effects determine the effective resistance of the coil; their contributions can only be approximated or simulated and in practice must be measured [16,17].

Consequently, in this study we compare the image SNR of coils that span a range of conductor losses measured on the bench. This work demonstrates that despite having higher resistance compared to standard thick copper, coils made of thinner or alternate conductors achieve SNRs that may exceed intuitive expectations. We believe this to be the first such exploration of a wide range of thicknesses (using 2 materials) with other variables carefully controlled.

2) Methods

Coil construction and bench measurements

Surface coils for a 0.48 T (20.56 MHz) system were constructed with different thicknesses of thin aluminum foil (9 μm , 13 μm , 20 μm , and 127 μm). The 9- and 13- μm -thick aluminum foils had a polyester laminate backing (~ 12 μm thick). Preliminary tests with small pieces of thinner aluminum (4 and 8 μm) without the backing material were challenging to work with, inconsistent and unreliable because they often had microscopic tears that impeded RF current flow. Thus, the resistance was higher than expected with these thin materials and they were not considered further. For comparison, coils were also constructed from thin copper (17 μm and 35 μm) with polyimide (Kapton, DuPont, Wilmington, DE) backing (~ 17 μm), self-adhesive copper tape (32 μm), and copper foil (127 μm). A much thicker copper coil was made of 600 μm copper bars to demonstrate bulky conductors. At this frequency the skin depths for copper and aluminum are 14.4 μm and 18.1 μm , respectively.

All coils consisted of a square 15×15 cm^2 loop of 6 mm wide traces with 12.5 cm long leads that were connected to a matching network (Figure 1). The long leads were used to create a coil that could be struck by a radiation treatment beam [14], whereas matching network components remained away from direct radiation. Total length of the trace was approximately $\lambda/18$ at 20.56 MHz which satisfies the maximum length criterion [18] without requiring additional capacitive breaks.

All coils (including 9- and 13- μm -thick aluminum foils with polyester backing) used thin acetate projector film for backing and structural support. The traces (6 mm wide) were cut manually from the copper and aluminum foils (including any backing) using a sharp blade, and

then fastened to the projector film using double-sided tape (3M 667-ESF, Saint Paul, MN, USA). For the 32 μm copper coil, 6-mm-wide copper tape (Venture Tape Corp. No. 1725, Rockland, MA, USA) was pressed onto the projector film in the same shape. Joints in the corners were soldered to create a continuous trace. The 600 μm bars were sheared from copper plate into 6 mm wide strips and then soldered into the required shape.

To ensure a stable electrical connection (especially for the aluminum coils that cannot be soldered) the ends of the leads were clamped between 2 pieces of FR4 PCB using nonmagnetic rivets. Two sets of 7-pin headers were soldered to the PCB enabling the coils to be connected to tuning and matching capacitors mounted on a separate PCB. The 600 μm copper coil was soldered to the PCB rather than riveted.

Each coil was made resonant near 20.56 MHz (Larmor frequency at 0.48 T) to measure quality factor (Q) and total inductance (L) by mating its pin headers to a temporary PCB with female headers connected to two capacitors in parallel (68 pF and 47 pF). The Q was determined as the ratio of the resonance frequency and the 3 dB bandwidth from the transmission spectrum obtained between 2 small (~ 1 cm \varnothing) pickup loops positioned at the corners of the square coils. Inductance (L) of each coil was determined from the measured resonant frequency (f) and the known fixed capacitance ($C = 115$ pF).

Measurements were conducted with a ZVL3 Vector Network Analyzer (VNA) (Rhode & Schwarz, Munich, Germany). The quality factor was measured both unloaded (coils supported by foam), and loaded by a head-sized, cylindrical aqueous phantom (19 cm \varnothing , 15 cm high, 55 mM NaCl and 5 mM NiCl₂) (ASG Superconductors, Genova, Italy). The unloaded Q was used to determine the resistive loss in each coil (R_c). Achievable SNR of a coil, relative to its intrinsic SNR ($i\text{SNR}$), is related to its efficiency ($\eta \in [0,1]$) by [19]

$$SNR = \sqrt{\eta} * iSNR. \quad (1)$$

Efficiency depends on loss contributions from the sample (R_s) and coil (R_c). There are additional losses introduced due to the capacitors, soldering, and radiative losses, but these losses cannot be readily separated from overall the resistive losses without modelling, [16] hence

$$\eta = 1 - \frac{R_C}{R_C + R_S}. \quad (2)$$

If $\eta < 1/2$ then coil losses are dominant, whereas if $\eta > 1/2$ the sample losses are dominant. Because all coils have the same geometry, except for conductor material and thickness, the intrinsic SNR is expected to be equal (i.e., R_S is the same for all coils).

A symmetric matching network (Figure 1, right) was built on a small PCB and connected to each coil through the headers. Tuning the coils to 20.56 MHz was achieved using a variable capacitor (Voltronics AJ55HV, 0–55 pF) and symmetrically-connected fixed capacitors (Voltronics D610, 150 pF). The coils were matched by adjusting a variable capacitor (Voltronics AJ25HV, 0–25 pF) connected in parallel with fixed capacitance (two 56 pF Voltronics D152 in series) by minimizing the return loss ($|S_{11}|$) at the resonance frequency measured with the VNA. To detune the coils during the transmission pulse of the imaging sequence, a passive crossed-diode (BAV 99) trap with a hand-wound inductor (~ 480 nH) was connected in parallel with the tuning capacitors. The coils were tuned and matched in the loaded condition.

Image SNR measurement

The constructed coils were tested in the Alberta 0.5 T linac-MR system [15]. This system is a combination of a modified clinical 0.48 T scanner (20.56 MHz ASG Superconductors) and a clinical linear accelerator. The parallel arrangement allows for real-time imaging while minimizing the effect of the Lorentz force on radiation dose distributions [15]. For each coil, a single, central 10-mm-thick slice of the cylindrical phantom was imaged (Figure 2) with a gradient-echo imaging sequence (field of view = 40×40 cm², TE = 12 ms, TR = 330 ms) to measure SNR variation with depth. A noise-only image corresponding to each signal image was acquired by repeating the same sequence without the excitation pulse. Each signal and noise image pair was acquired 3 times. Identical positioning of the phantom and all coils was assisted by markings on the table and phantom. Furthermore, transmit and receive RF amplifier gain settings were kept consistent across all measurements. This was achieved by controlling these parameters within the TNMR spectrometer software (TECMAG, Houston, TX, USA) of the system. Raw k-space data from the TNMR software was fast Fourier transformed in MATLAB (MathWorks, Natick, MA, USA).

The SNR profile as a function of depth from the surface of the phantom was determined to compare image quality across a large portion of the phantom. Stepping pixel by pixel along the

depth axis of the phantom, at each depth the pixel values for the central 16 mm of the phantom were averaged to determine a mean signal value for that depth. The noise magnitude for each profile was determined by taking the standard deviation of the corresponding noise-only image. The ratio of the signal values at each depth and the noise for that image gave an SNR profile for each signal and noise image pair. The SNR profiles for the three image pairs for each coil were averaged to give a single profile for comparison to those of the other coils.

As the standard for comparison of SNR between coils, locally weighted smoothing was applied to the SNR profile of the 127 μm copper coil using the *smooth* function in MATLAB (local regression, 2nd degree polynomial, based on nearest 10 points). Each coil profile was fitted to this standard curve by multiplication with a scaling constant obtained using least squares (LSQCURVEFIT, MATLAB, MATHWORKS). The scaling constant corresponds to the relative SNR which gives the minimum least squared error between the scaled standard and the data. The goodness of the fit was analyzed using χ^2 and p-values (χ -square test) [20]. Here the P-value is the chance that, assuming the fit is correct, a data set could be obtained and give a higher χ -square. Extremely low p-values ($\ll 0.01$) signify poor fits. A p-value very close to 1 (> 0.99) suggests overfitting, or overestimated data errors. The solution covariance was used to determine the 95% confidence range which was used as the error in the relative SNR [20].

The relationship between the relative coil SNR as determined above, and the coil efficiency, as determined previously through bench measurements, was used to obtain an intrinsic SNR for this coil setup by fitting the SNR and root of efficiency data to Equation 1.

3) Results

Coil Efficiency

The coil efficiency as a function of conductor thickness is tabulated for aluminum and copper in Supporting Information Table S1. As can be expected [3], the quality of the coils (Supporting Information Table S1) improves with increased conductor thickness, and aluminum coils have a lower efficiency than copper coils for a similar thickness. These bench measurements predict that even the thinnest (9 μm) aluminum conductor coil will achieve an SNR that is almost 75% of that of the 127 μm copper foil coil, despite a 3 times higher coil resistance.

Image SNR

Figure 2b,c show example images acquired with the 9 μm thick aluminum coil and the 127 μm thick copper coil. Images acquired using each coil look qualitatively similar despite the wide variation in coil materials, thereby showing that other variables such as geometry were tightly controlled. In Figure 3, the SNR profiles for each coil (averaged from 3 measurements) are shown to highlight the SNR differences between different thicknesses and materials. Figure 4 shows the SNR of each coil (squares and diamonds) relative to that of the 127 μm copper coil as a function of conductor thickness. The 95% confidence interval for the fit values is around 2% making the error bars too small to visualize. The p-value is between 0.4 and 0.5 which confirms fits and statistical assumptions are reasonable [20].

The general trend in SNR as a function of thickness and material is similar to the trend predicted by differences in coil resistance and efficiency. Indeed, plotting the image SNR and bench measured efficiency (Figure 5) shows qualitative agreement.

4) Discussion

As predicted, both bench measurements and acquired images confirm that the type and the thickness of conductor affect the achievable SNR. By carefully controlling experimental variables the bench-measured prediction of SNR ratios and the achieved image SNR ratios agree within uncertainty for most coils. The difference exceeded uncertainty in only in two cases (17 μm copper and 13 μm aluminum), for which the uncertainties are likely underestimated.

The calculated efficiency (Supporting Information Table S1) demonstrates that at 0.5 T for head-sized phantoms the coils are operating in a transition region between sample-dominated losses (R_S) and coil-dominated losses (R_C). Despite the range in unloaded Q (Supporting Information Table S1), all of the tested copper coils have efficiency greater than 0.5. This is reflected in the SNR measurements where the best and worst copper coils differ by about 20% despite the dramatic difference in thickness. The same is true for the 127 μm aluminum coil. However, for aluminum the range of thicknesses extends to very thin coils where conductor losses are greater than the sample losses. This is illustrated by the performance of the 9 μm aluminum coil which is strongly coil-loss dominated ($\eta = 1/3$). Still, this coil is in the range ($\eta > 0.25$) where the slope (Figure 5) remains below 1. In terms of SNR performance, this results in only a 35% difference between the 127 μm copper coil and the 9 μm aluminum coil.

The 32 μm copper coil is an outlier because it outperforms most other foil coils despite being of intermediate thickness. This coil's traces are machine-cut strips of copper tape and hence have likely overall smoother edges than were achieved by cutting copper and aluminum foil manually with a sharp blade. Edge imperfections (roughness) lead to additional losses because at these frequencies there is current crowding near high-curvature points of the conductor. Current will be especially concentrated at the edges of the cross-section where the imperfections are.

Overall, the measurements indicate that whereas a thickness of multiple skin depths certainly yields the best-performing RF coils, the losses increase only modestly down to thicknesses on the order of 1 skin depth. The losses nearly double between 127 μm and 20 μm thick aluminum (a factor of 5 smaller thickness), but it only takes a further halving of conductor thickness to 9 μm to increase losses by the same amount again. The data in Figure 4 indeed suggest the appearance of an elbow in the SNR performance near 20 μm .

These data are also an experimental exploration of the theoretical relationships in Eqs. 1 and 2 [19]. Impacts of material and thickness are lumped together in the total resistance of each coil, or its efficiency. The data are in general agreement with the expected relationship (Figure 5). The minimal SNR advantage of the thickest copper (600 μm bars) over the 127 μm standard illustrates that covering a wider range of possible efficiencies will require changes beyond simply the thickness of the conductors (e.g., coil dimensions, capacitor distribution, and/or frequency). The measurements would consequently be more challenging to control and compare.

These measurements were performed at an intermediate field strength of 0.5 T. As field strength (and consequently resonant frequency) increases, the proportion of losses due to the load will increase. At higher field strengths, even thin aluminum coils are expected to operate in the sample-loss-dominated regime; thus, the use of this material in coils for, e.g., PET-MR scanners, is quite feasible.

5) Conclusions

As MRI technology seeks to use RF coils made of thin or alternate conductors for emerging applications, there has been a need to investigate conductors that are lossier than traditional bulky copper conductors. This study presents a verification of the efficiency and SNR relationship for identically-constructed coils under controlled conditions. The coils cover a nearly five-fold range of losses and use the same lumped components and loading conditions for all coils. As expected,

the losses due to thin conductors are most dramatic when they are thinner than one skin depth at the Larmor frequency. Furthermore, for thick coils the effect of using aluminum rather than copper is found to be minimal when comparing conductors of similar thickness. A 127 μm thick aluminum coil, despite its 20% higher resistance, achieves the same SNR as a 127 μm copper foil conductor. Even coils with several times higher losses ($3\times$ higher resistance) achieve SNR better than half that of thick copper and aluminum (65% that of 127 μm copper foil).

These results highlight the fact that a significant change in coil resistance may not lead to a catastrophic loss of SNR, thus justifying the use of thin or alternate conductors in applications where a limited SNR loss is not critical and outweighed by the advantages gained, such as comfort or radiological transparency (e.g., aluminum).

6) Acknowledgements

Technical support was provided by ASG Superconductors. We thank Emmanuel Blosser and Cory Lambert for assistance with the Alberta Linac-MR, and Lance Spiridon and Curtis Osinchuk for fabricating mechanical components. We acknowledge funding from Natural Sciences and Engineering Research Council (NSERC), Alberta Cancer Foundation (ACF), Alberta Innovates, and Canadian Institutes of Health Research (Grant No. CIHR MOP 93752). Special thanks to Alberta Health Services (AHS) for their continued support of the Alberta Linac-MR project.

7) References

1. Serway RA, Jewett JW. Physics for scientists and engineers. 6th ed. Thomson-Brooks/Cole; 2004.
2. Hoult DI, Richards RE. The signal-to-noise ratio of the nuclear magnetic resonance experiment. *J. Magn. Reson.* 1976;24:71–85 doi: 10.1016/0022-2364(76)90233-X.
3. Giovannetti G, Francesconi R, Landini L, et al. Conductor geometry and capacitor quality for performance optimization of low-frequency birdcage coils. *Concepts Magn. Reson. Part B Magn. Reson. Eng.* 2004;20B:9–16 doi: 10.1002/cmr.b.20005.
4. Corea JR, Flynn AM, Lechêne B, et al. Screen-printed flexible MRI receive coils. *Nat. Commun.* 2016;7:10839 doi: 10.1038/ncomms10839.
5. Gruber B, Rehner R, Laistler E, Zink S. Anatomically Adaptive Coils for MRI—A 6-Channel Array for Knee Imaging at 1.5 Tesla. *Front. Phys.* 2020;8:80 doi: 10.3389/fphy.2020.00080.
6. Vincent JM, Rispoli J V. Conductive Thread-Based Stretchable and Flexible Radiofrequency Coils for Magnetic Resonance Imaging. *IEEE Trans. Biomed. Eng.* 2020;67:2187–2193 doi: 10.1109/TBME.2019.2956682.
7. Zhang D, Rahmat-Samii Y. A Novel Flexible Electrotextile 3T MRI RF Coil Array for Carotid Artery Imaging: Design, Characterization, and Prototyping. *IEEE Trans. Antennas Propag.* 2019;67:5115–5125 doi: 10.1109/TAP.2019.2891700.
8. Port A, Luechinger R, Brunner DO, Pruessmann KP. Conductive Elastomer for Wearable RF Coils. In: *Proc. Intl. Soc. Mag. Reson. Med 26. Virtual Conference; 2020.* p. 1137.
9. Mehmman A, Varga M, Vogt C, et al. On the Bending and Stretching of Liquid Metal Receive Coils for Magnetic Resonance Imaging. *IEEE Trans. Biomed. Eng.* 2019;66:1542–1548 doi: 10.1109/TBME.2018.2875436.
10. Malko JA, McClees EC, Braun IF, Davis PC, Hoffman JC. A flexible mercury-filled surface coil for MR imaging. *Am. J. Neuroradiol.* 1986;7:246–247.
11. Nordmeyer-Massner JA, De Zanche N, Pruessmann KP. Stretchable coil arrays: Application to knee imaging under varying flexion angles. *Magn. Reson. Med.* 2012;67:872–879 doi: 10.1002/mrm.23240.
12. Rieke V, Ganguly A, Daniel BL, et al. X-ray compatible radiofrequency coil for magnetic resonance imaging. *Magn. Reson. Med.* 2005;53:1409–1414 doi: 10.1002/mrm.20494.
13. Sander CY, Keil B, Chonde DB, Rosen BR, Catana C, Wald LL. A 31-channel MR brain array

coil compatible with positron emission tomography. *Magn. Reson. Med.* 2015;73:2363–2375 doi: 10.1002/mrm.25335.

14. Barta R, Ghila A, Rathee S, Fallone BG, De Zanche N. Impact of a Parallel Magnetic Field on Radiation Dose Beneath Thin Copper and Aluminum Foils. *Biomed. Phys. Eng. Express* 2020;6:037002.

15. Fallone BG. The Rotating Biplanar Linac–Magnetic Resonance Imaging System. *Semin. Radiat. Oncol.* 2014;24:200–202 doi: 10.1016/J.SEMRADONC.2014.02.011.

16. Giovannetti G, Hartwig V, Landini L, Santarelli MF. Classical and lateral skin effect contributions estimation in strip MR coils. *Concepts Magn. Reson. Part B Magn. Reson. Eng.* 2012;41 B:57–61 doi: 10.1002/cmr.b.21210.

17. Giovannetti G, Fontana N, Monorchio A, Tosetti M, Tiberi G. Estimation of losses in strip and circular wire conductors of radiofrequency planar surface coil by using the finite element method. *Concepts Magn. Reson. Part B Magn. Reson. Eng.* 2017;47B:e21358 doi: 10.1002/cmr.b.21358.

18. Chen C-N (Ching-nien), Hoult DI. *Biomedical magnetic resonance technology* / C-N. Chen and D.I. Hoult. Bristol: A. Hilger; 1989.

19. Edelstein WA, Glover GH, Hardy CJ, Redington RW. The intrinsic signal-to-noise ratio in NMR imaging. *Magn. Reson. Med.* 1986;3:604–618.

20. Aster RC, Borchers B, Thurber CH. *Parameter estimation and inverse problems*. 2nd ed. Academic Press; 2013.

Figures

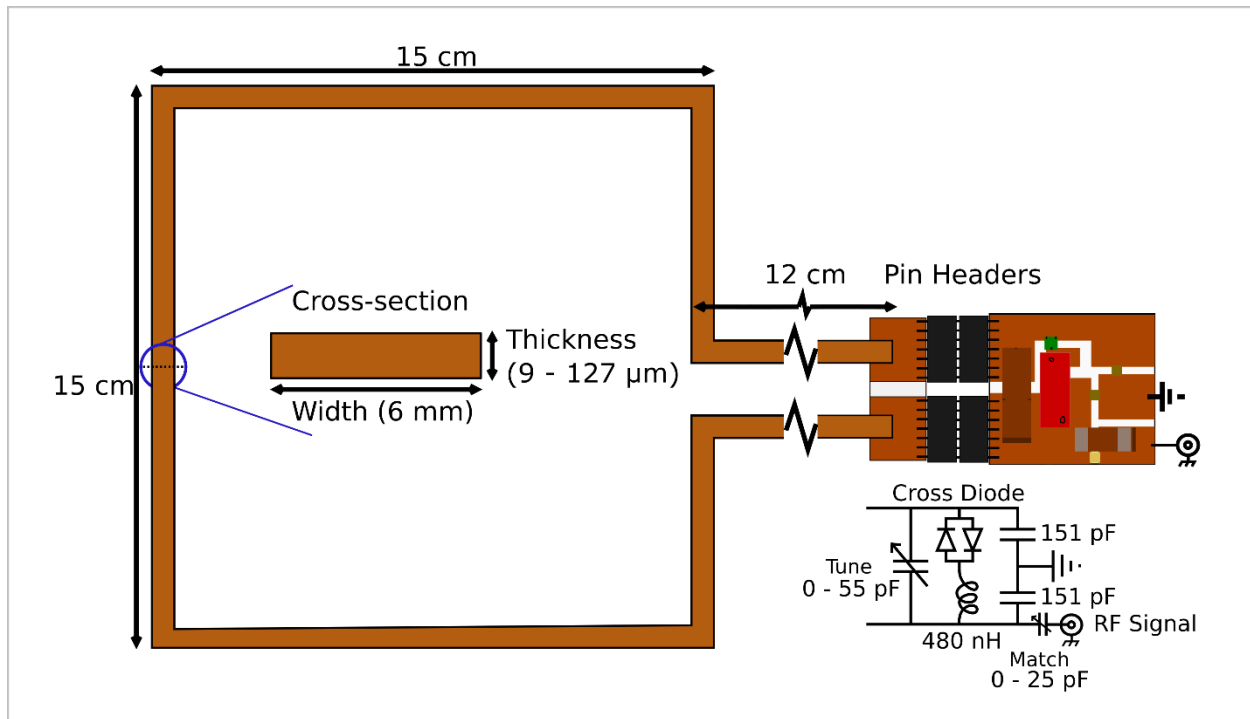


Figure 1: Coil schematic showing the dimensions ($15 \times 15 \text{ cm}^2$) of the conducting loop, as well as the layout of the tuning and matching circuits on the PCB and corresponding circuit diagram.

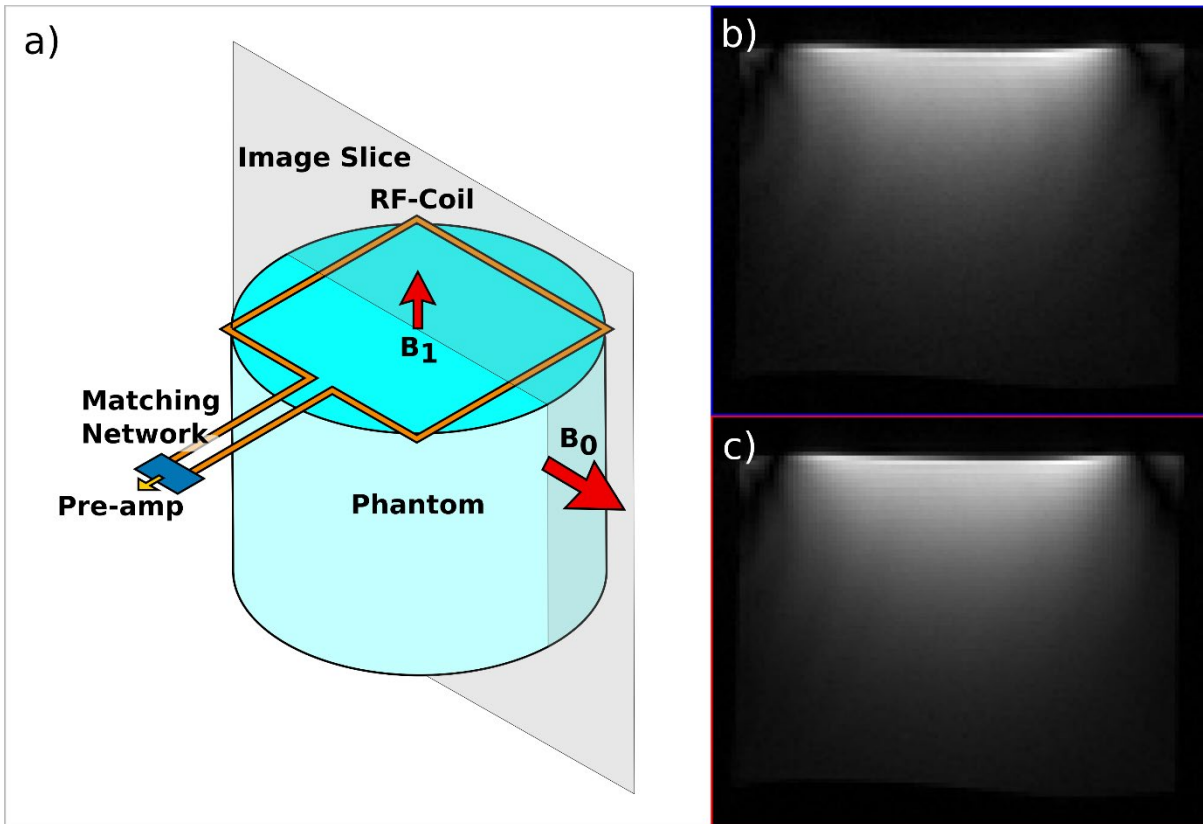


Figure 2: Experimental setup used for acquisition of phantom images in the linac-MR (2a, left) as well as sample images for the 9 μm aluminum (2b, top right) and 127 μm copper coils (2c, bottom right).

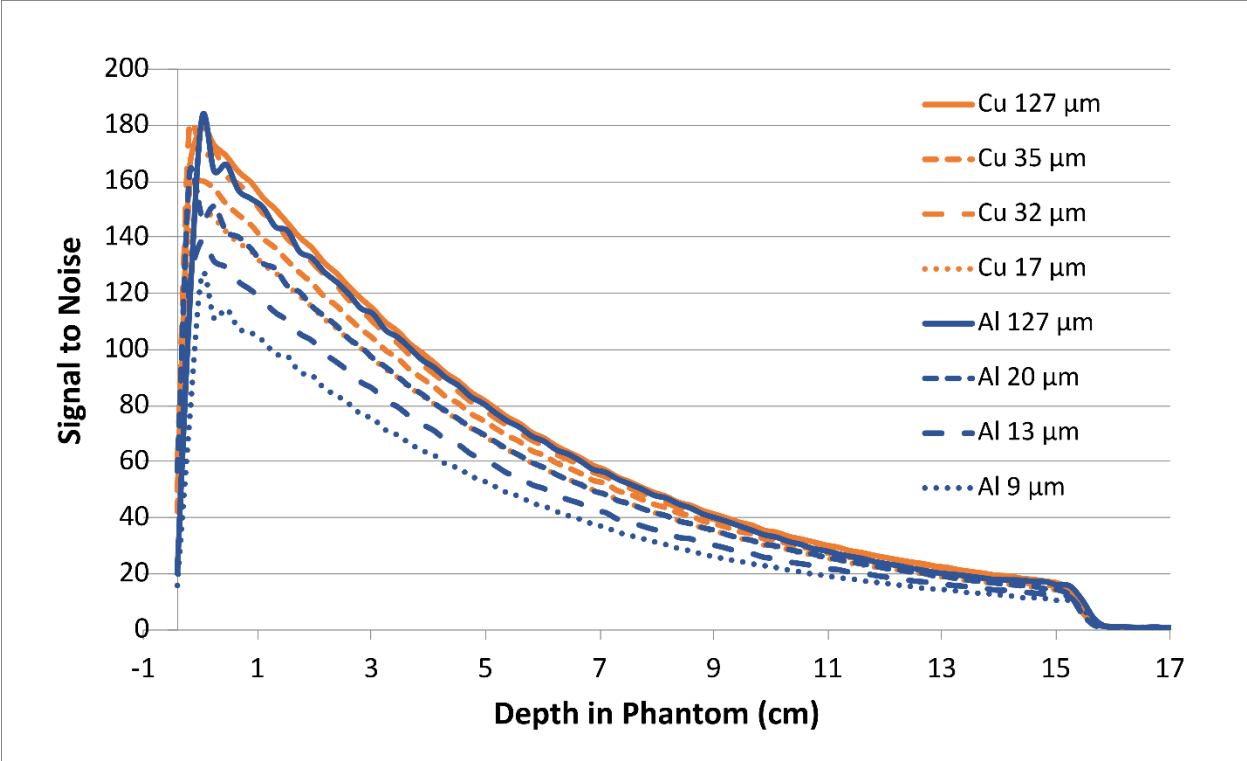


Figure 3: The averaged SNR image profiles for each RF coil. Data for the 600 μm thick copper coil is omitted because it was acquired with a different scaling.

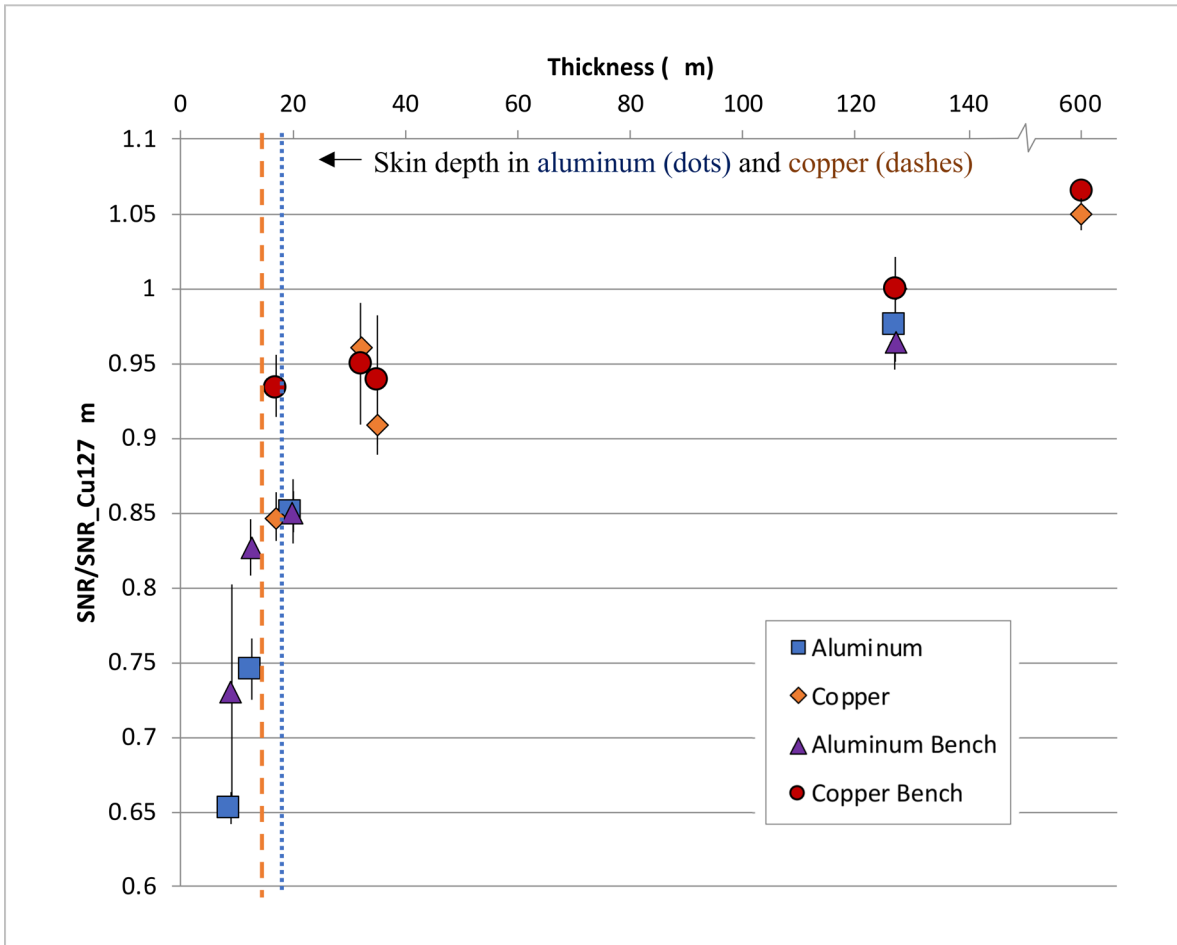


Figure 4: SNR relative to that of the 127 μm copper coil from both the images and bench measurements. Mean load impedance of the phantom was $0.41+j0.19 \Omega$.

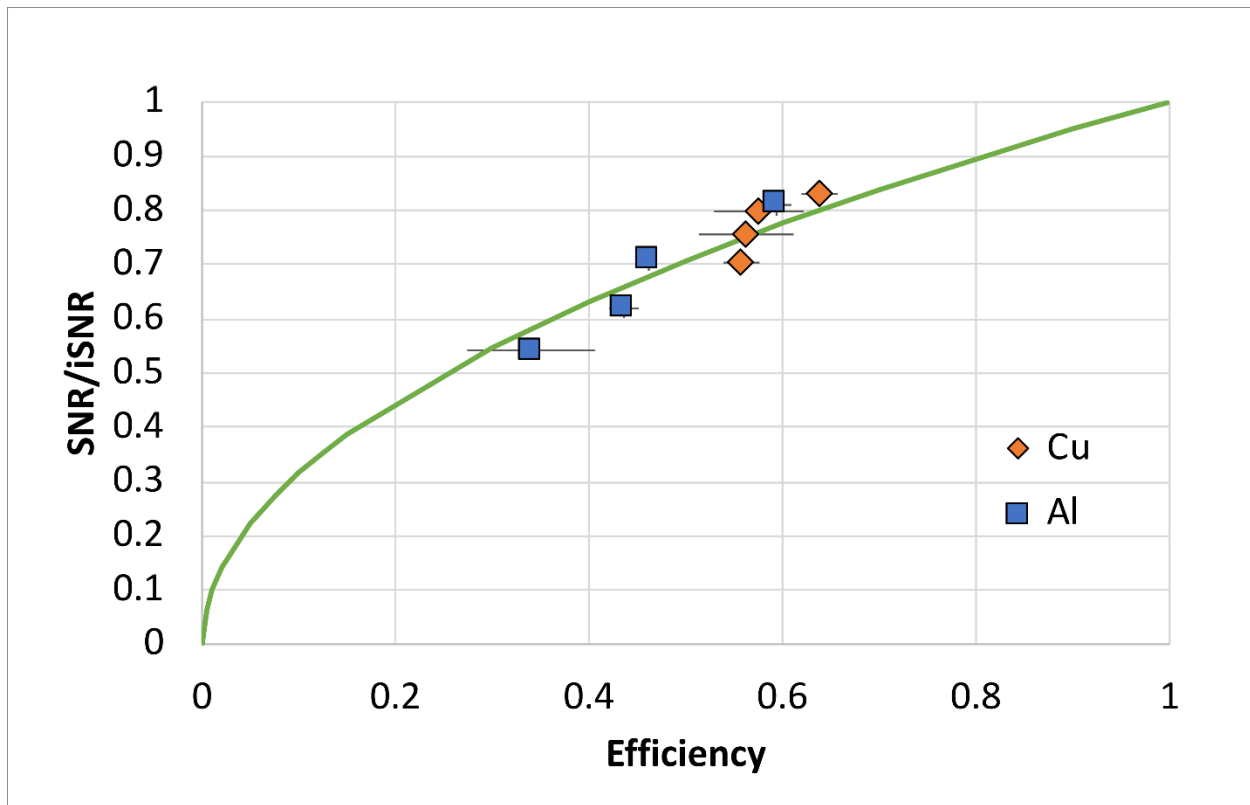


Figure 5: The measured image SNR/iSNR plotted against the bench measured efficiency (η). The curve is the relationship given by Eq. 1 and iSNR is obtained by fitting.

Aluminum	Resistance (Ω)	Unloaded	Loaded	Ratio	Efficiency
127 μm	$.286 \pm 0.009$	239 ± 8	97 ± 2	2.5 ± 0.1	0.59 ± 0.02
20 μm	$.462 \pm 0.007$	149 ± 1	80.0 ± 0.5	1.86 ± 0.02	0.461 ± 0.006
13 μm	$.570 \pm 0.009$	114 ± 1	64 ± 2	1.77 ± 0.05	0.44 ± 0.02
9 μm	$.74 \pm 0.01$	89 ± 1	59 ± 6	1.5 ± 0.2	0.34 ± 0.07
Copper					
600 μm	$.172 \pm 0.003$	390 ± 5	104 ± 2	3.76 ± 0.08	0.734 ± 0.006
127 μm	$.24 \pm 0.01$	290 ± 10	104 ± 2	2.8 ± 0.1	0.64 ± 0.02
35 μm	$.30 \pm 0.02$	230 ± 10	100 ± 10	2.3 ± 0.3	0.56 ± 0.05
32 μm	$.29 \pm 0.02$	230 ± 10	99 ± 9	2.4 ± 0.3	0.58 ± 0.05
17 μm	$.33 \pm 0.01$	205 ± 8	90.6 ± 0.5	2.3 ± 0.1	0.56 ± 0.02

Supporting Information Table S1 - Bench measurements of coil resistance, unloaded and loaded Q and efficiency. Mean load impedance of the phantom was $0.41 + j0.19 \Omega$. The range of resonant frequencies was 20.1 to 21.3 MHz.